LOCAL AND GLOBAL VIBRATION ANALYSIS OF THIN-WALLED MEMBERS SUBJECTED TO INTERNAL FORCES – APPLICATION OF GENERALISED BEAM THEORY

Rui A.S. Bebiano*[1], Dinar R.Z. Camotim[1], Rodrigo M. Gonçalves[2]

[1]Instituto Superior Técnico, Technical University of Lisbon, Lisbon, Portugal
{rbebiano,dcamotim}@civil.ist.utl.pt

[2]Universidade Nova de Lisboa, Lisbon, Portugal
rodrigo.goncalves@fct.unl.pt

Keywords: Thin-Walled Members, Generalized Beam Theory (GBT), Vibration of Loaded Members, Local Vibration, Global Vibration.

Abstract. *This paper presents the results of a comparative study on the effects of various internal forces/moments on the vibration behaviour of thin-walled members. The analyses are based on Generalised Beam Theory (GBT), a thin-walled bar theory which accounts for cross-section in-plane deformations – its main distinctive feature is the representation of the member deformed configuration by means of a linear combination of cross-section deformation modes multiplied by the corresponding longitudinal amplitude functions. The study concerns simply supported cold-formed steel lipped-channel cold-formed steel members exhibiting a wide range of lengths and subjected to four uniform internal force/moment diagrams: (i) axial force, (ii) major-axis bending moment, (iii) minor-axis bending moment and (iv) bi-moment – their magnitudes are specified as percentages of the corresponding critical (buckling) values. The influence of the internal force/moment diagrams (applied loadings) on the member vibration behaviour is assessed in terms of the (i) the frequency drop and (ii) changes in the vibration mode shape. The GBT-based results, obtained with the code GBTUL 2.0 (developed by the authors and available online) are validated by means of available analytical formulae and values provided by analyses carried out by means of the ANSYS and CUFSM codes.*

1   INTRODUCTION

It is well known that, owing to the high slenderness of their walls, thin-walled structural systems exhibit responses that may be governed by phenomena involving local and/or distortional deformations of their member cross-section. Moreover, it is common practice to analyse the vibration behaviour of such systems under the (approximate) assumption that they are not subjected to any loading (*i.e.*, are load-free). However, structural systems members are invariably subjected to loadings of more or less significant magnitude and, therefore, the associated geometrically non-linear effects (global, local or distortional), may have some impact on their natural vibration frequencies and mode shapes.

Over the last decades, several studies have been published concerning the vibration behaviour of thin-walled members acted by axial forces (*e.g.*, [1-3]) and/or bending moments (*e.g.*, [4-6]). However, the vast majority of these works are restricted to members vibrating in *global* modes, *i.e.*, involving exclusively bending and/or torsional deformations. Only a few (and quite recent) publications deal with the local/distortional vibration of loaded thin-walled members − practically all of them concerning members under axial force only, *i.e.*, columns (*e.g.*, [7-8]).

Generalised Beam Theory (GBT) (*e.g.*, [9]) is an original thin-walled bar theory that differs from their counterparts mainly due to the fact that the description of the member behaviour is based on structurally meaningful cross-section deformation modes with amplitudes varying along the member length. In recent years, the authors employed GBT to analyse the vibration behaviour of thin-walled members acted under axial forces [10] and (uniform or non-uniform) bending moments [11]. However, no comparison is available the relative influence of the various internal forces and moments on the member vibration behaviour.

The objective of this work is to present a GBT-based comparative study concerning the local and/or global vibration behaviour of thin-walled members acted by uniform (i) axial force, (ii) major-axis bending moment, (iii) minor-axis bending moment and (iv) bi-moment diagrams. Both the free-vibration and buckling behaviours (under the 4 loadings) are first analysed, since their knowledge is indispensable to assess the loaded member vibration behaviour. The analyses are carried out for lipped channel members exhibiting a wide length range and subjected to several loading levels, defined as percentages of the corresponding critical bifurcation values. The influence of the loading is assessed through the (i) natural frequency values and (ii) vibration mode shapes. The results presented and discussed were obtained with GBTUL 2.0, a user-friendly GBT-based code available online [12], and are validated by means of values provided by available analytical formulae and/or numerical analyses performed with the codes ANSYS [13] or CUFSM [14].

2.   GENERALISED BEAM THEORY – BRIEF OVERVIEW

As mentioned above, GBT is a one-dimensional bar theory that expresses/discretizes the member deformed configuration as a linear combination of cross-section *deformation modes* multiplied by the corresponding (modal) amplitude functions. A very brief overview of this theory is presented next − a complete account can be found in references [9-11].

In GBT, the mid-plane displacement field components − along axial ($x − u(x,s)$), plate midline ($s − v(x,s)$) and plate normal ($z − w(x,s)$) directions − are expressed as

$$u(x,s) = u_k(s)\phi_{k,x}(x) \qquad v(x,s) = v_k(s)\phi_k(x) \qquad w(x,s) = w_k(s)\phi_k(x) \qquad (1)$$

where (i) functions $u_k(s)$, $v_k(s)$ and $w_k(s)$ define the cross-section deformation mode k, (ii) function $\phi_k(x)$ (or $\phi_{k,x}(x)$) is the corresponding longitudinal amplitude function and (iii) the summation convention applies to subscript k. The first step of any GBT-based structural analysis consists of determining the cross-section deformation modes and determining the associated mechanical properties − this is be done through a systematic procedure termed *Cross-Section Analysis* [9],

based on a given cross-section discretisation into N_d natural and intermediate nodes. Fig. 1 illustrates this procedure for a lipped channel steel (E=210GPa, v=0.3, ρ=7.8t/m^3) member: (i) cross-section geometry (Fig. 1(a)) and nodal discretisation (Fig. 1(b)), and (ii) in-plane and out-of-plane deformed shapes of the first 10 (out of N_d) deformation modes (Figs. 1(c$_1$)-(c$_2$)) – their exhibit global (**1-4**), distortional (**5-6**) or local (**7-10** – null warping displacements) natures. The results presented and discussed in this work concern members with this cross-section and having various lengths.
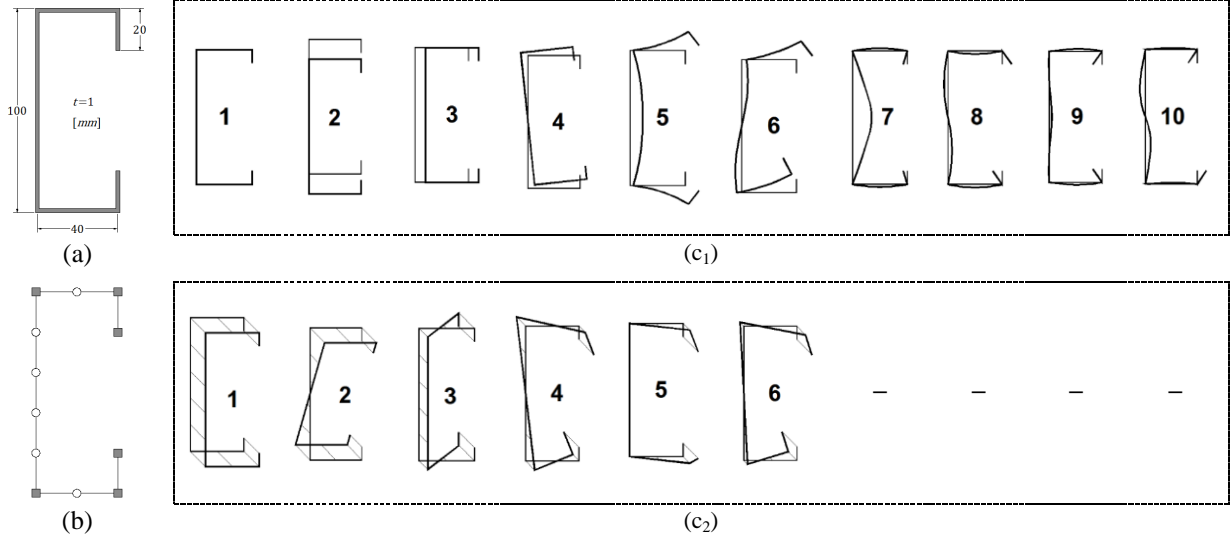

Figure 1: Lipped channel cross-section (a) geometry, (b) nodal discretisation and (c) GBT global (**1-4**), distortional (**5-6**) and local (**7-10**) deformation modes – (c$_1$) in-plane ($v_k(s)$, $w_k(s)$) and (c$_2$) out-of-plane ($u_k(s)$) deformed shapes.

Depending on the particular problem under consideration, only a selected fraction of the N_d deformation modes obtained needs to be included in the GBT analysis ($1 \leq n_d \leq N_d$), thus leading to a reduction in the number of degrees of freedom involved. The next step consists of performing the *Member Analysis*, which consists of solving the vibration eigenvalue system (of dimension n_d)

$$\left[C_{ik}\phi_{k,xxxx} - D_{ik}\phi_{k,xx} + B_{ik}\phi_k + W_j X_{jik}\phi_{k,xx} \right] - \omega^2 \left[R_{ik}\phi_k - Q_{ik}\phi_{k,xx} \right] = 0 \tag{2}$$

together with the associated boundary conditions, to determine natural frequencies ω (eigenvalues) and the corresponding vibration mode shapes (eigenfunctions, expressed as combinations of the modal amplitude functions). In this system, (i) C_{ik}, D_{ik} and B_{ik} are linear stiffness matrices, (ii) Q_{ik} and R_{ik} are mass matrices, and (iii) X_{jik} are geometric stiffness matrices, associated with the acting axial normal stress (σ_{xx}) resultants W_j, namely $W_1 \equiv N$, $W_2 \equiv M_Y$, $W_3 \equiv M_Z$, $W_4 \equiv M_\omega$.

In simply supported members, Eq. (2) provides the first $N_v \equiv n_d$ natural vibration modes, which are combinations of exactly sinusoidal modal functions $\phi_k(x)$, and associated natural frequency values. A simple way of quantifying the participation of a given deformation mode i on the configuration of a vibration mode is through the respective modal participation factor P_i, defined as

$$P_i = \int_L |\phi_i(x)| dx \Big/ \sum_{k=1}^{n_d} \int_L |\phi_k(x)| dx \tag{3}$$

3. LOAD-FREE VIBRATION BEHAVIOUR

The curves depicted in Fig. 2(a) show the variation of the *load-free* lipped channel member first three natural frequencies ($\omega_1 \equiv \omega_f$, ω_2 and ω_3) with the length L, all displayed in bi-logarithmic scale – results provided by GBT analyses including the n_d=10 deformation modes depicted in Figs. 2(c$_1$)-(c$_2$). For validation, Fig. 2(a) also includes ω_f values obtained from (i) ANSYS shell finite element analyses and, for minor-axis *flexural vibration* only, (ii) the analytical expression (*e.g.*, [15])

$$\omega_f = (\pi/L)^2 \sqrt{(EI_3)/(\rho A)} \tag{4}$$

where A and I_3 are the member cross-section area and minor moment of inertia. Moreover, Fig. 2(b) provides the GBT modal participation diagram concerning the member fundamental vibration mode shapes. Finally, Figs. 2(c_1)-(c_2) show the ANSYS fundamental vibration mode shapes of the members with $L=100\,cm$ and $L=200\,cm$. These results prompt the following remarks:

(i) The three natural frequencies decrease monotonically with L and tend to zero as L goes to infinity. The ω_1 and ω_2 curves are very close for $150 \le L \le 500\,cm$ – they intersect at $L \approx 400\,cm$, a length for which the natures of these two vibration modes switch. For $L>400\,cm$, mode **3** becomes clearly dominant, which explains why the ω_f-L curve virtually coincides with the dashed one, yielded by Eq. (4) – differences below 0.1%. Moreover, the GBT and ANSYS are in perfect agreement (differences below 2.5%) – note, however, that the SFEA involve 2000-15000 d.o.f., while the GBT analyses require only 10 (*i.e.*, a 0.07%-0.5% fraction).

(ii) The modal participation diagram shows that the fundamental vibration mode shape is (ii_1) *local* (mode **7** prevails), for $L<25\,cm$ (very short members), (ii_2) *distortional* (mode **5** governs, but relevant contributions from modes **3** and **7**), for $25<L<120\,cm$ (see Fig. 2(c_1)) (ii_3) *flexural-torsional-distortional* (modes **2**, **4** and **6**), for $120<L<400\,cm$ (see Fig. 2(c_2)) and (ii_4) *purely flexural* (only mode **3**), for $L>400\,cm$.
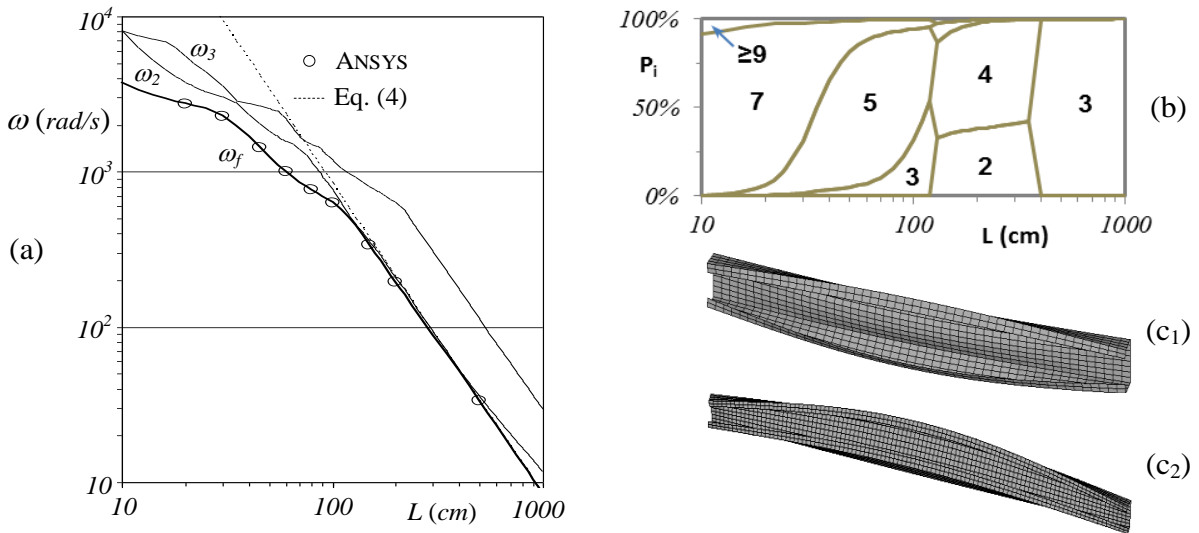

Figure 2: Load-free member vibration behaviour: (a) variation of ω_f, ω_2 and ω_3 with L, (b) GBT modal participation diagram for the fundamental modes and (c) vibration mode configurations for (c_1) $L=100\,cm$ and (c_2) $L=200\,cm$

4. BUCKLING BEHAVIOUR

4.1 Column Buckling

Figure 3(a) shows the uniformly compressed member (column) buckling curves associated with (i) single half-wave ($N_{b.1}$-L) and (ii) critical (N_{cr}-L) instability modes – Figs. 3(c_1)-(c_2) depict the corresponding modal participation diagrams (P_i-L). As for Fig. 3(b), it provides 3D a representation of the $L=100\,cm$ columns critical mode. These results lead to the following conclusions:

(i) The $N_{b.1}$-L curve exhibits two minima: (i_1) $N_{b.1}(8cm)=23.3\,kN$ (outside the figure) and (i_2) $N_{b.1}(65cm)=62.94\,kN$ – in both cases, the CUFSM results are within 0.2%. The N_{cr}-L and $N_{b.1}$-L curves only differ for $10 \le L \le 210\,cm$ – the former has a $N_{cr} \approx 23.3\,kN$ horizontal plateau.

(ii) The single half-wave buckling modal participation diagram shows these buckling mode natures, for progressively larger lengths: *local* (modes **7+9**), *mostly distortional* (**3+5+7**), *flexural-torsional* (**2+4**) and *flexural* (**3**). Note that local buckling (**7+9**) is only critical up to

L=210cm (Fig. 5(b) shows the L=100cm column buckling mode, with n_h=13 half-waves). For higher L values the two diagrams rigorously coincide (single half-wave critical modes).

(iii) It is worth noting that the single half-wave column buckling modes are *practically identical* to the load-free vibration modes – compare Figs. 2(c_1) and 3(c_1). This feature, which was unveiled and explained in [10], is valid for simply supported members and stems from the approximate proportionality of the inertia and geometric (for compression) matrices.
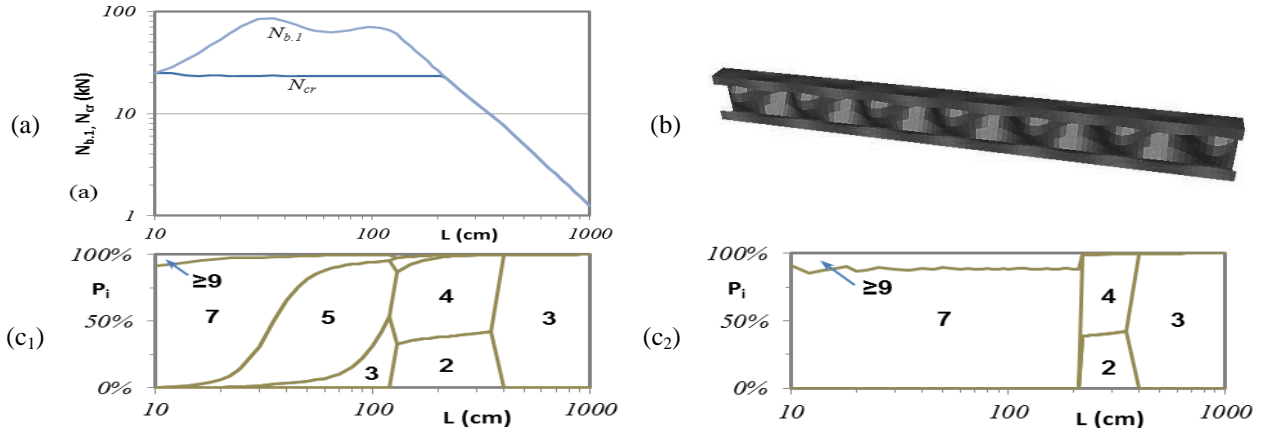
(a)

(b)

(c_1)

(c_2)

Figure 3: Column buckling behaviour: (a) buckling curves (N_b-L, N_{cr}-L), (b) L=100cm columns critical buckling mode and (c) modal participation diagrams of the (c_1) single half-wave and (c_2) critical buckling modes

4.2   Beam Buckling

This section addresses the lipped channel buckling behaviour under (i) major and (ii) minor axis bending – the applied moments cause compression on the top flange and web, respectively. Figs. 4(a_1)-(a_2) show the critical buckling curves $M_{Y.cr}$-L and $M_{Z.cr}$-L, while figures 4(b_1)-(b_2) display the associated modal participation diagrams. Figs. 4(c_1)-(c_2) depict the critical buckling modes of L=100cm beams acted by M_Y and M_Z. These buckling results lead to the following comments:
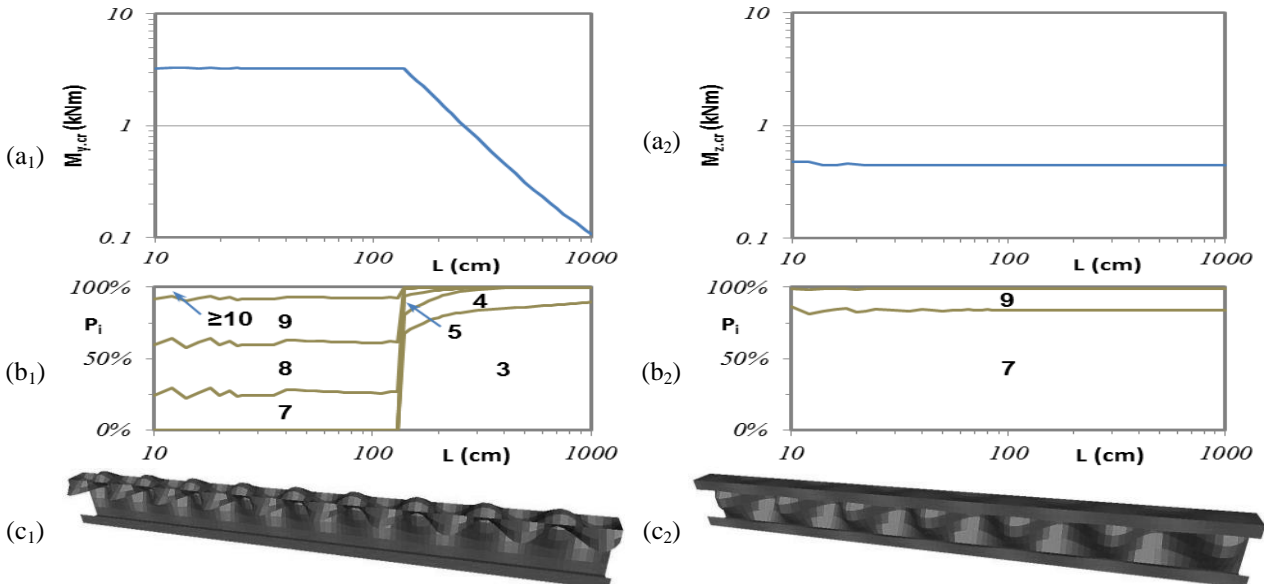
(a_1)

(a_2)

(b_1)

(b_2)

(c_1)

(c_2)

Figure 4: Beam buckling behaviour: (a) buckling curves (a_1) $M_{Y.cr}$-L and (a_2) $M_{Z.cr}$-L), (b_1)-(b_2) corresponding modal participation diagrams and (c) L=100cm critical buckling mode unde (c_1) major-axis and (c_2) minor-axis bending

(i)   The $M_{Y.cr}$-L curve has a $M_{Y.cr}$≈3.25kNm horizontal plateau up to L=130cm and descends monotonically to zero afterwards. On the other hand, the $M_{Z.cr}$-L curve is practically a hori-

zontal line ($M_{Z.cr}$=0.444 kNm) for $10 \leq L \leq 1000\,cm$. The CUFSM estimates of these critical buckling moments only by about 0.6% ($M_{Y.cr}$) and 0.1% ($M_{Z.cr}$).

(ii) The major-axis bending modal participation diagram reveals two critical buckling mode natures: (ii$_1$) *local* buckling (modes **7-9**) for $10 \leq L \leq 130\,cm$ and (ii$_2$) *flexural-torsional-distortional* buckling (**3-5**) for $L>130\,cm$ – while the former involves a half-wave number increasing with L, up to n_h=24 (see Fig. 4(c$_1$) – n_h=19), the latter is always single half-wave.

(iii) The minor-axis bending modal participation diagram shows that, regardless of the length, all beams buckle in local modes that always combine contributions from modes **7** (predominant) and **9**, and exhibit a half-wave number that increases with L – Fig. 4(c$_2$) depicts the L=100 cm beam buckling mode (n_h=13).

4.3   Buckling under Bi-moment

Finally, the lipped channel buckling behaviour under a uniform bi-moment diagram is investigated. Figs. 5(a)-(b) display the critical buckling curve $M_{\omega cr}$-L and the associated modal participation diagram. Fig. 5(c) shows provides the L=40 cm member critical buckling mode. From the observation of these results, it is possible to conclude that:

(i) Like in the beams under minor-axis bending, the critical buckling bi-moment values are practically independent of L, *i.e.*, $M_{\omega cr}$-L is a horizontal line within the range considered ($M_{\omega cr} \approx 0.04\,kNm^2$) – the corresponding CUFSM differs by about 1.25%.

(ii) The modal participation diagram indicates that the critical buckling modes are local, combining major contributions participations from deformation modes **7-10** with minor (but not negligible) ones from additional higher-order local modes ($\geq$**10**), and exhibit increasing half-wave numbers. The L=40 cm member buckling mode shape, shown in Fig. 5(c), evidences the fact that deformations only occur at the upper lip and adjacent flange region (where the compressive stresses caused by the bi-moment diagram are larger).
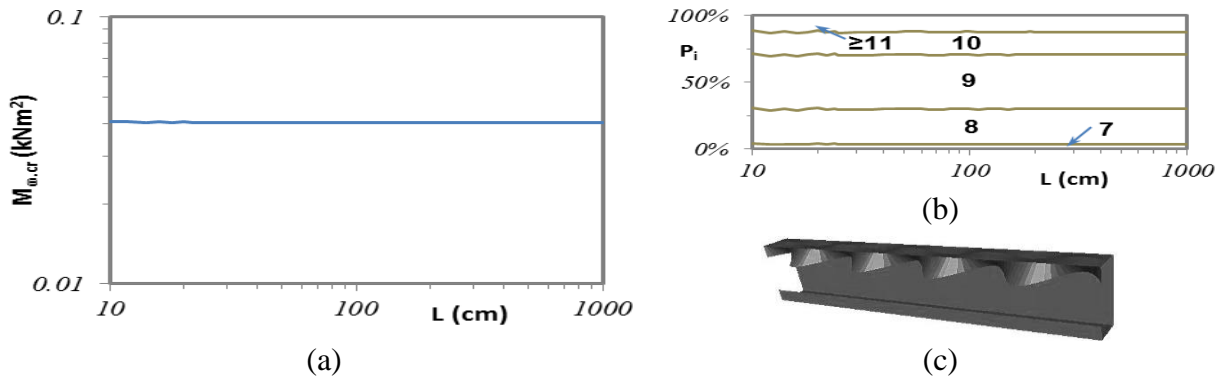

Figure 5: Buckling behaviour of a member acted by a bi-moment diagram: (a) buckling curve $M_{\omega cr}$-L, (b) modal participation diagram and (c) L=40 cm member critical buckling mode.

5.   LOADED MEMBER VIBRATION BEHAVIOUR

5.1   Column Vibration

The influence of the compressive force N on the member vibration behaviour is analysed in this section – the compression level is quantified as a fraction α of the corresponding critical buckling value, *i.e.*, N=αN_{cr}. The curves in Fig. 6(a) provide the variation of the fundamental frequency $\omega_{f.\alpha}$ with L, for 9 α values: α=0 (unloaded member), 0.1, 0.25, 0.5, 0.75, 0.9, 0.95, 0.99, 0.999. As for Figs. 6(b$_1$)-(b$_4$), they show the modal participation diagrams associated with vibration modes corresponding to α=0.5, 0.75, 0.95, 0.999. These results prompt the following remarks:

(i) As expected, the $\omega_{f.\alpha}$-L curve moves down as α increases. Up to α=0.5, the curves remain parallel and fairly close to the initial load-free one (ω_f-L), according to the relation [10]

$$\beta = \sqrt{1-\alpha} \qquad (5)$$

where $\beta = \omega_{f.\alpha}/\omega_f$ − this relation is valid as long the column vibration mode (associated with $\omega_{f.\alpha}$) exhibits a single half-wave. This ceases to hold true for (i_1) $\alpha \geq 0.75$ and (i_2) $L \leq 210\,cm$, situation for which the curves becomes visibly more irregular. Furthermore, for $\alpha \geq 0.95$ the $\omega_{f.\alpha}$ drops become more pronounced until, ultimately (for α=1), one has $\omega_{f.\alpha}$=0 (when looking at Fig. 6(a) recall that $\omega_{f.\alpha}$ is plotted in logarithmic scale − the same applies for Figs. 7(a), 8(a) and 9(a)) − a well-known classical result, which can now be generalised to vibration modes involving local and/or distortional deformation.

(ii) The nature of the column vibration modes is not altered below α=0.5 (even if $\omega_{f.\alpha=0.5} < \omega_f$) − note that modal participation diagrams in Figs. 2(b) and 6(b_1) coincide. However, for α=0.75 the modal diagram changes slightly within the range $16 \leq L \leq 30\,cm$ (see Fig. 6(b_2)).

(iii) As α approaches 1, the vibration mode participation diagram changes continuously (see Figs. 6(b_3)-(b_4)): the GBT modes **7+9** become progressively more dominant for the $L \leq 210\,cm$ members. The vibration modes associated with α=0.999 are virtually identical to the column critical buckling modes, as can be observed by comparing Figs. 3(c_2) and 6(b_4).
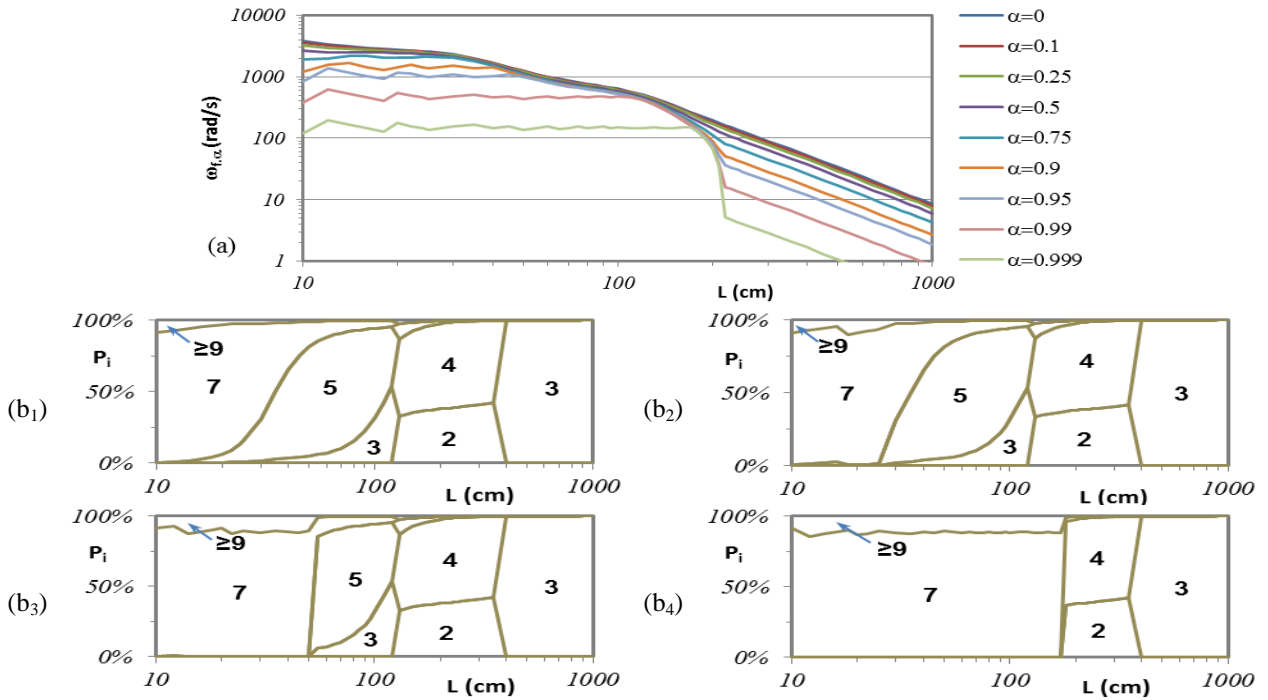

Figure 6: Column vibration behaviour: (a) ω_α-L curves for α=0, 0.1, 0.25, 0.5, 0.75, 0.9, 0.95, 0.99, 0.999 and (b_1)-(b_4) modal participation diagrams for α=0.5, 0.75, 0.95, 0.999.

5.2 Beam Vibration

The influence of major and minor-axis bending moment on the member vibration behaviour is now investigated. Concerning M_Y, the applied moment level is again quantified by α, i.e., $M_Y = \alpha M_{Y.cr}$. The $\omega_{f.\alpha}$-L curves shown in Fig. 7(a) correspond, once more, to α=0 (load-free member) and 0.1, 0.25, 0.5, 0.75, 0.9, 0.95, 0.99, 0.999. Figs. 7(b_1)-(b_4) show the modal participation diagrams associated with α=0.1, 0.75, 0.95, 0.999. The observation of these vibration results leads to the following conclusions:

(i) The applied bending moment causes frequency drops that (i$_1$) are imperceptible for $\alpha \leq 0.25$ and (i$_2$) become very significant (and abrupt) for $\alpha \geq 0.95$. In qualitative terms, the $\omega_{f.\alpha}$-L curves resemble their column counterparts (compare Figs. 6(a) and 7(a)) – however, the frequency drops are more pronounced for the columns.

(ii) The comparison between the modal participation diagrams in Figs. 2(b) and 7(b$_1$) shows that, unlike the natural frequency, the fundamental vibration mode shape may be considerably altered even by the presence of quite small applied moments (α=0.1) – in fact, either (ii$_1$) the distortional mode **6** joins modes **5+7** (intermediate beams) or (ii$_1$) the global mode **3** joins modes **2+4** (longer beams – they are completely separated for α=0). Inside the 0.1<α<0.95 range (Figs. 7(b$_2$)-(b$_3$)), (ii$_1$) modes **8-10** progressively replace mode **7** (short beams), (ii$_2$) the contributions of modes **5** and **6** become closer (intermediate beams) and (ii$_2$) the relevance of mode **2** gradually fades (longer beams). Finally, for $\alpha \geq 0.95$ the vibration mode shapes change drastically, approaching their critical buckling mode counterparts – for α=0.999, the beam fundamental vibration and critical buckling modes virtually coincide throughout the whole length range (compare Figs. 4(b$_1$) and 7(b$_4$)).
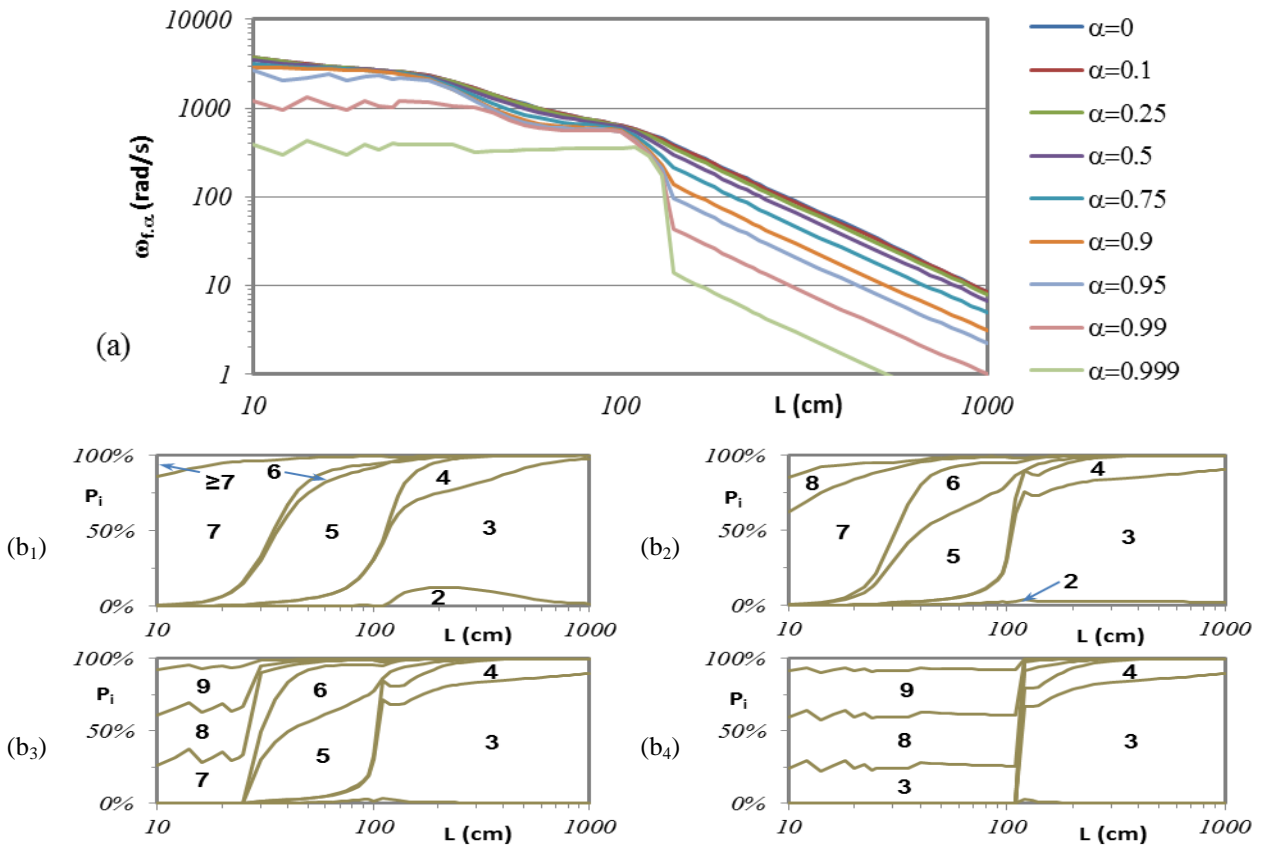
Figure 7: Major-axis beam vibration behaviour: (a) ω_α-L curves for α=0,0.1,0.25,0.5,0.75,0.9,0.95, 0.99 and 0.999; (b$_1$)-(b$_4$) modal participation diagrams for α=0.1,0.75,0.95 and 0.999

Figure 8(a) concerns beam under minor-axis bending ($M_Z=\alpha M_{Z.cr}$) and the $\omega_{f.\alpha}$-L curves displayed correspond to the same 9 α values as before. Figs. 8(b$_1$)-(b$_4$) present the modal participation diagrams associated with α=0.1, 0.5, 0.95, 0.999. It is observed that:

(i) The $\omega_{f.\alpha}$-L curves are considerably different from those obtained previously for columns (Fig. 6(a)) or beams under major-axis bending (Fig. 7(a)), which lie below the ω_f-L curve (*i.e.*, $\omega_{f.\alpha \neq 0}<\omega_{f.\alpha=0}$) for the whole length range. Indeed, the $\omega_{f.\alpha}$-L curves concerning minor

axis bending eventually merge with the load-free curve (*i.e.*, $\omega_{f.\alpha\neq0}\approx\omega_{f.\alpha=0}$ for lengths higher than a given value, which increases with α).

(ii) The modal participation diagram for α=0.1 shows no change with respect to its load-free counterpart. However, for α=0.5, the fundamental vibration modes cease to exhibit major-axis flexure and torsion − in fact, the GBT modes **2+4**, which prevailed within the load-free 130≤L≤400cm range, are replaced by minor-axis flexure and distortion (modes **3+5**).

(iii) For higher α values, GBT modes **7+9** gradually replace the above combinations of modes **3+5** − *i.e.*, for short beams the fundamental vibration and critical buckling modes (see Fig. 4(b$_2$)) are now identical − for α=0.999, the predominance of modes **7+9** already extends up to L=210cm. Unlike for major-axis bending, the "transformation" of the beam vibration mode shape into its buckling counterpart (iii$_1$) is now almost instantaneous (there is no gradual transition) and (iii$_2$) "spreads" along the length range as α increases.
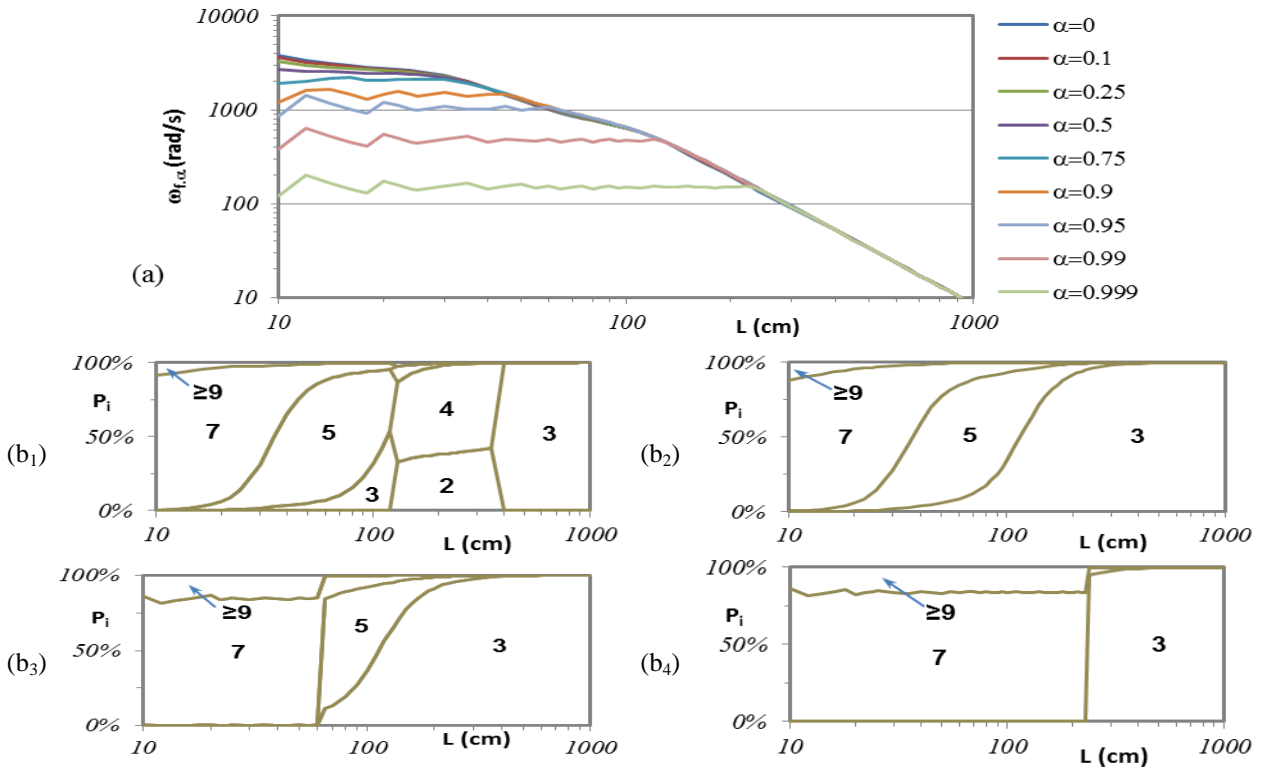

Figure 8: Minor-axis beam vibration behaviour: (a) ω_α-L curves for α=0, 0.1, 0.25, 0.5, 0.75, 0.9, 0.95, 0.99, 0.999 and (b$_1$)-(b$_4$) modal participation diagrams for α=0.1, 0.5, 0.95, 0.999.

5.3   Vibration under Bi-moment

Finally, the vibration behaviour of beams subjected to bi-moments is addressed. Fig. 9(a) shows $\omega_{f.\alpha}$-L curves concerning the same 9 α values as before ($M_\omega = \alpha M_{\omega.cr}$). Figs. 9(b$_1$)-(b$_4$) display the modal participation diagrams of the member vibration modes for α=0.1, 0.75, 0.99, and 0.999. The observation of these results leads to the following conclusions:

(i) As somehow expected, following the buckling results presented in sub-sections 4.2 and 4.3, the $\omega_{f.\alpha}$-L curves concerning members subjected to bi-moments are qualitatively similar to those reported earlier for beams under minor-axis bending − for a given L value, which increases with α, each curve merges with the load-free curve (ω_f-L). However, frequency drops only become sizeable for quite high loading levels (α≥0.95).

9

(ii) The presence of a quite small bi-moment (*e.g.*, α=0.1) produces a noticeable change in the vibration mode nature, clearly visible in Fig. 9(b$_1$). In qualitative terms, such change is similar to that experienced by the beams under major-axis bending, shown in figure 7(b$_1$) – the only noticeable difference is the lesser role played now by mode **3** in the $120 \leq L \leq 400\,cm$ range, which is "compensated" by the added predominance of modes **2+4**.

(iii) As α increases, the mode nature keeps changing visibly: (iii$_1$) for $30 \leq L \leq 95\,cm$, mode **6** emerges and combines equitably with mode **5**, and (iii$_2$) for $95 \leq L \leq 400\,cm$, mode **5** "joins" the mode **2+3+4** (with increasing relevance of mode **3**) – see Fig. 9(b$_2$).

(iv) Finally, for very high α values ($\alpha \gtrsim 0.95$), the mode combination **7-11**, which characterises the member buckling modes, "spreads" rapidly along the length as α increases (see Figs. 9(b$_3$)-(b$_4$)). However, note that, even for α=0.999, the modal participation diagram of the vibration modes is still quite different its critical buckling mode counterpart (see Fig. 5(b)) – in particular the maximum half-wave numbers remain very far apart (22 and 223, respectively).
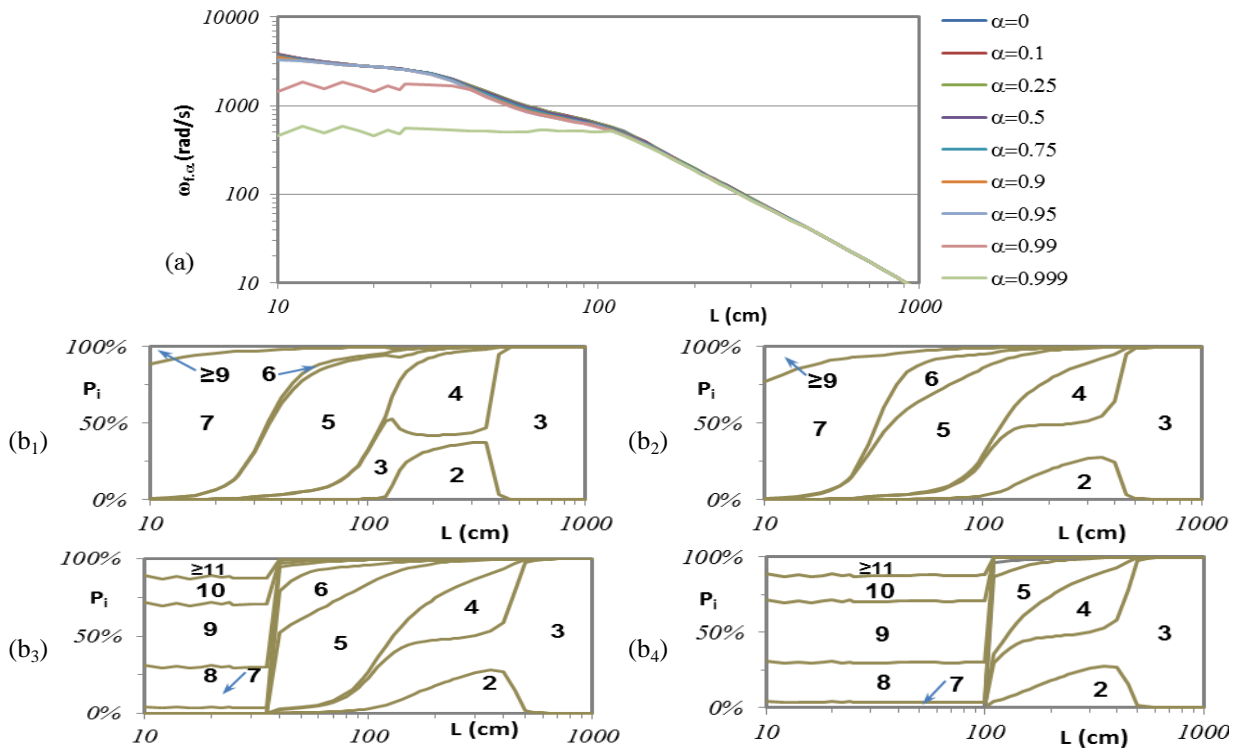

Figure 9: Vibration behaviour of members subjected to bi-moments: (a) ω_α-L curves for α=0, 0.1, 0.25, 0.5, 0.75, 0.9, 0.95, 0.99, 0.999 and (b$_1$)-(b$_4$) modal participation diagrams for α=0.1, 0.75, 0.99, 0.999

5.5   Comparative Assessment

Figures 10(a)-(d) plot the variation of $\beta = \omega_{f,\alpha}/\omega_f$ with α plots for members with (i) L=30cm, (ii) L=100cm, (iii) L=250cm and (iv) L=500cm acted by the four loading types considered in this work. Also shown is the curve defined by Eq. (5), valid for columns buckling in single half-wave modes. These curves make it possible to assess quantitatively the *load-sensitivity* of the member vibration behaviour – in particular, the sensitivity of the fundamental frequency with respect to the applied load level. The joint observation of these figures leads to the following conclusions:

(i) For all lengths, the curve corresponding to compression (N) is always below those associated with the remaining loading types – this is because uniform compression causes the most severe member stiffness degradation. The curve stemming from Eq. (5) either (i$_1$) overestimates significantly the column natural frequency load-sensitivity (L=30cm and L=100cm), or

(i_2) matches it almost perfectly (L=150cm and L=500cm) – this discrepancy is due to the fact that the latter two columns buckle in single half-wave modes (unlike the former two).

(ii) The curves concerning beams under major-axis bending are relatively similar to their column counterparts – the former always lie below the latter. The similarity increases with the length, which explains why the differences are only marginal (they do not exceed 5%) for L=250cm and L=500cm – this means that, for this length range, Eq. (5) also provides reasonably good estimates of the fundamental natural frequency drop in beams under major-axis bending.

(iii) Except for L=30cm, the curves concerning members subjected to minor-axis bending or bi-moment are fairly similar – the latter always lie below the former and, as in the previous item, the similarity increases with the length (they are indistinguishable for L=500cm). For L=30cm the M_Z and N curves are very close, which is due to the fact that the uniformly compressed web triggers the instability of both members – for this length, the M_ω curve lies well above its M_Z counterpart. As the length increases, both the M_Z and M_ω curves (iii_1) tend to 1.0 for $0 \leq \alpha < 1.0$, and (iii_2) fall very abruptly to zero in the close vicinity of α=1 – i.e., the fundamental natural frequency of the "not too short" members subjected to minor-axis bending or bi-moment is almost *load-insensitive*.
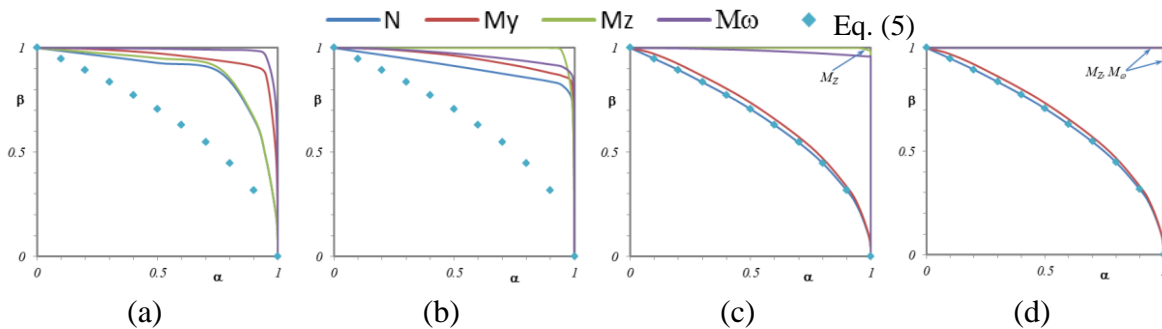

Figure 10: Load-sensitivity of the natural frequency of members with lengths (a) L=30cm, (b) L=100cm, (c) L=250cm and (d) L=500cm that are subjected to compression (N), major (M_Y) and minor (M_Z) axis bending, and bi-moment (M_ω).

6. CONCLUSION

This work reported an investigation, carried out by means of analyses based on Generalised Beam Theory (GBT), dealing with the influence of four uniform internal force/moment diagrams (N, M_Y, M_Z and M_ω) on the fundamental vibration behaviour of thin-walled lipped channel members. Various loading levels, expressed as percentages of the member critical buckling loads/moments, were considered and the load-sensitivities of the member fundamental natural frequency and vibration mode shape (taking advantage of the GBT modal features) were assessed in detail.

Table 1 summarises (and compares qualitatively) the influence exerted by the above four internal forces/moments on the lipped channel member (i) fundamental frequency drop and (ii) vibration mode shape change) – it is worth noting that both these influences are also heavily dependent on the particular member length (or vibration mode nature). Generally speaking, it may be argued that the loading that causes the largest fundamental frequency drop is the one for which the corresponding vibration mode shape changes the least.

Table 1: Comparation between the effects produced by the four applied loadings (N, M_Y, M_Z, M_ω)

Effect	+ ⟵			
Fundamental frequency drop	N	M_Y	M_ω	M_Z
Vibration mode shape change	M_ω	M_Y	M_Z	N

ACKNOWLEDGMENTS

REFERENCES

[1] F. de Borbón and D. Ambrosini, On free vibration analysis of thin-walled beams axially loaded. *Thin-Walled Structures*, **48**(12), 915-920, 2010.

[2] T.P. Vo and J. Lee, Free vibration of axially loaded thin-walled composite Timoshenko beams. *Archive of Applied Mechanics*, **81**(9), 1165-1180, 2011.

[3] J. Banerjee, S. Fisher, Coupled bending-torsional dynamic stiffn. matrix for axially loaded beam elements. *Intern. J. for Numerical Methods in Engineering*, **33**(4), 739-751, 1992.

[4] A. Joshi and S. Suryanarayan, Unified analytical solutions for various boundary conditions for the coupled flexural-torsional vibration of beams subjected to axial loads and end moments. *Journal of Sound and Vibration*, **129**(2), 313-326, 1989.

[5] A. Joshi and S. Suryanarayan, Iterative method for coupled flexural-torsional vibration of initially stressed beams. *Journal of Sound and Vibration*, **146**(1), 81-92, 1991.

[6] C.F. Shih, J. Chen and J. Garba, Vibration of large space beam under gravity effect. *AIAA Journal*, **24**(7), 1213-1216, 1986.

[7] M. Ohga, K. Nishimoto, T. Shigematsu and T. Hara, Natural frequencies and mode shapes of thin-walled members under in-plane forces. *Thin-Walled Structures – Research and Development*, N. Shanmugam, J. Liew and V. Thevendran (eds.), Elsevier, 501-508, 1998.

[8] M. Okamura and Y. Fukasawa, Characteristics of instability of local vibration of thin-walled members under periodic axial forces. *Structural and Earthquake Engineering* (*JSCE*), **15**(2), 215-223, 1998.

[9] D. Camotim, C. Basaglia, R. Bebiano, R. Gonçalves and N. Silvestre, Latest developments in the GBT analysis of thin-walled steel structures. *Stability and Ductility of Steel Structures* (*SDSS'Rio 2010* – Rio de Janeiro, 8-10/9), E. Batista *et al.* (eds.), 33-58, 2010.

[10] N. Silvestre and D. Camotim, Vibration behaviour of axially compressed cold-formed steel members, *Steel and Composite Structures*, **6**(3), 221-236, 2006.

[11] R. Bebiano, N. Silvestre and D. Camotim, Local and global vibration of thin-walled members subjected to compression and non-uniform bending, *Journal of Sound and Vibration*, **315**(3), 509-535, 2008.

[12] R. Bebiano, D. Camotim, R. Gonçalves, N. Silvestre, *GBTUL 2.0 – Buckling and Vibration of Thin-Walled Members* (2013), freeware available at: http://www.civil.ist.utl.pt/gbt/

[13] ANSYS Inc., *ANSYS® Academic Research*, Release 8.1.

[14] Z. Li and B.W. Schafer, Buckling analysis of cold-formed steel members with general boundary conditions using CUFSM: conventional and constrained finite strip methods, *Proceedings of the 20th International Specialty Conference on Cold-Formed Steel Structures* St. Louis, USA, 2010.

[15] R. Clough and J. Penzien, *Dynamics of Structures* (2nd ed.), McGraw-Hill, New York, 1993.